13C-1H Heteronuclear dipolar correlation studies of the hydrogen bonding of the quinones in Rhodobacter sphaeroides R26 RCs

Rossum, B.J. van; Liemt, W.B.S. van; Gast, P.; Lugtenburg, J.; Groot, H.J.M. de

^{13}C-^{1}H Heteronuclear Dipolar Correlation Studies of the Hydrogen Bonding of the Quinones in *Rhodobacter sphaeroides* R26 Reaction Centers

B. J. van Rossum[1], W. B. S. van Liemt[1], P. Gast[2], J. Lugtenburg[1],
and H. J. M. de Groot[1]

[1] Gorlaeus Laboratories, Leiden Institute of Chemistry and [2] Huygens Laboratories,
Leiden Institute of Physics, Leiden University, Leiden, The Netherlands

Abstract. The photosynthetic reaction center (RC) of the photosynthetic bacterium *Rhodobacter sphaeroides* R26 contains two quinones, Q_A and Q_B. Solid-state heteronuclear (^{1}H-^{13}C) dipolar correlation spectroscopy has been used to study the binding of the quinones in the ground state for RCs reconstituted with 1-^{13}C ubiquinone-10. Lee–Goldburg cross-polarization buildup curves are recorded to determine distances r_{CH} between the 1-^{13}C carbon labels and the protons involved in the polarization transfer. The 1-^{13}C of both Q_A and Q_B have intermolecular correlations with protons that resonate downfield, in the region of hydrogen-bonding protons. The distances between the carbon labels and the correlated protons are short, 0.21 ± 0.01 nm. Hence the nuclear magnetic resonance provides evidence for strong hydrogen-bonding interactions at the 1-C=O of both Q_A and Q_B for RCs in the ground state. The environment of the 1-^{13}C of the Q_B is structurally heterogeneous compared to that of the Q_A. The data can be reconciled with a strong H-bonding interaction of the 1-C=O of Q_A with Ala M260 NH, and with complex hydrogen bonding involving NH of Ile-L224 and of Gly-L225, and possibly the Ser-L223 hydroxyl group of the 1-C=O of the Q_B, in the proximal site.

1 Introduction

The primary processes of photosynthesis in the photosynthetic bacterium *Rhodobacter sphaeroides* R26 comprise a light-induced charge separation by which excitation energy is converted into chemical energy. The charge-separation process occurs in the photosynthetic reaction center (RC), a large transmembrane protein complex consisting of three polypeptide chains, the L, M, and H subunits that support nine cofactors (Fig. 1) [1]. Upon excitation with light, an electron is transferred from the special pair P via the accessory chlorophyll B_A and bacteriopheophytin Φ_A to the primary quinone Q_A. The largest free energy change is associated with the reduction of Q_A and accounts primarily for the 30–40% loss in photochemical energy conversion in the RC [2]. Within about 200 µs the
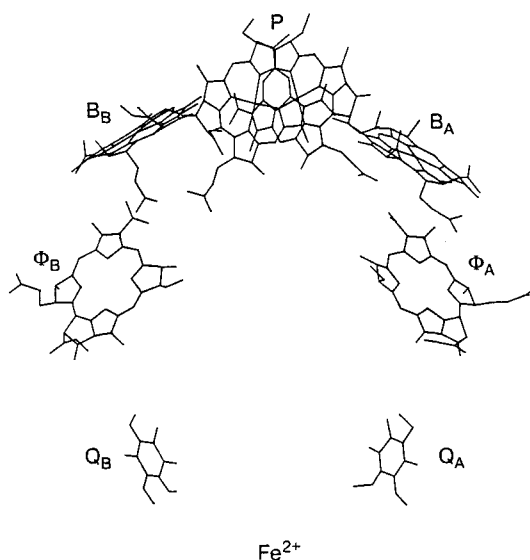
Fig. 1. Arrangement of the cofactors in the *R. sphaeroides* R26 RC.

electron is transferred to the secondary quinone Q_B. After a second excitation, Q_B is doubly reduced and doubly protonated and is released from the RC as a Q_BH_2 diquinol. Although Q_A and Q_B are both identical ubiquinone-10 (UQ_{10}) molecules (Fig. 2), their electrochemical function and binding properties are different. While Q_A is tightly and permanently bound to the protein, it temporarily accepts single electrons and serves as a one-electron gate. Q_B, on the other hand, is weakly bound. During the photosynthesis process it accepts two electrons and is chemically converted in the RC. To resolve the mechanisms behind the molecular electronics of the photosynthetic charge separation process, the characterization of differences in quinone–protein interactions between the Q_A and Q_B, and differences in binding between the neutral and the reduced forms of the quinones is important.
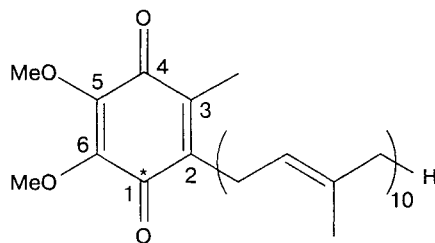

Fig. 2. Structure of UQ_{10} and IUPAC numbering scheme of the UQ_{10} ring system.

^{13}C cross-polarization magic-angle spinning nuclear magnetic resonance (CP MAS NMR) spectroscopy of *Rb. sphaeroides* R26 RCs reconstituted with [1-^{13}C] UQ_{10} or [4-^{13}C] UQ_{10} for Q_A, revealed highly asymmetric interactions of the carbonyls with the protein in the ground state [3]. While the [1-^{13}C] Q_A R26 RC MAS NMR provided narrow lines with a short CP time, both at low temperatures $210 \leq T \leq 250$ K from frozen detergent-solubilized and precipitated preparations, and at ambient temperatures from precipitated samples, a [4-^{13}C] Q_A signal could be observed only in partially hydrated samples at temperatures $T \leq 255$ K and for longer CP times of about 3 ms [3, 4]. The good CP efficiency and a narrow NMR signal provide convincing evidence for a tight fit at the 1-^{13}C=O Q_A, which indicates strong hydrogen bonding at this carbonyl functionality with an isotropic shift of the 1-^{13}C=O very similar to the shift observed for unbound UQ_{10}, in the solid state or in solution [3].

Electron–nuclear double resonance measurements and Q-band electron paramagnetic resonance (EPR) spectroscopy on $Q_A^{\cdot-}$ also show a pronounced asymmetry between both carbonyl positions in the semiquinone state, however with the stronger binding at the 4-C=O [5–9]. From electron spin echo envelope modulation (ESEEM) measurements on Zn-substituted RCs, it was inferred that the $N\delta_1$ of the imidazole ring of His M219 is involved in a hydrogen-bonding interaction to the 4-C=O of $Q_A^{\cdot-}$ [10]. In addition, ESEEM and EPR spectroscopy on Zn-substituted RCs, in combination with site-directed mutagenesis, provided evidence for additional weaker hydrogen bonding between the 1-^{13}C=O of the $Q_A^{\cdot-}$ and the peptide nitrogen of Ala M260 [11]. Finally, in the reduced $P^+Q_A^{\cdot-}$ state, librational motion of the ring has been detected with an axis over the carbonyl carbons [12].

Quinone carbonyls of both the Q_A and Q_B in native RCs from *R. sphaeroides* have been investigated extensively with FTIR and asymmetric hydrogen bonds for Q_A and symmetric hydrogen bonds for Q_B have also been inferred from IR isotope-edited fingerprint spectra of RCs reconstituted with specifically labeled ubiquinone [13–16]. In line with the EPR, the absence of a shift of the mode dominated by the 1-C=O Q_A vibration was interpreted as an essentially free or weakly bound carbonyl group. There is converging evidence that the light-induced formation of the donor-acceptor charge pair, $P^+Q_A^{\cdot-}$, and the forward electron transfer from $Q_A^{\cdot-}$ to Q_B induce charge-compensating relaxation rearrangements accompanying conformation movements within the protein [17–22]. In addition, different conformation states involving proximal and distal Q_B positions were identified after crystallization of the RCs under dark and light conditions leading to the concept of conformational gating of the $Q_A^{\cdot-}Q_B$ to $Q_AQ_B^{\cdot-}$ electron transfer [23, 24]. Vibrational spectroscopy favors a unique Q_B binding site in the wild type and a number of mutants [25–27]. These studies have confirmed that both carbonyls of neutral Q_B are engaged in comparable interactions with the protein. This fits the description of the proximal binding site for neutral Q_B [28].

In line with the librational motion detected with EPR, the NMR responses of the [4-^{13}C] carbonyl and the adjacent [5-^{13}C] in Q_A were attributed to dynamic Q_A–protein interactions [3, 29]. In addition, a shortening of T_1^ρ for hydrated-pre-

cipitated [4-^{13}C] Q$_A$ RCs was observed for temperatures approaching $T \approx 255$ K from below, indicating characteristic frequencies around 50–60 kHz for the restricted dynamics at the 4-C=O side [4]. It was observed that the line width of the label response was highly sensitive to the degree of hydration of the precipitated RCs. A narrow [4-^{13}C] Q$_A$ response was only observed for a "wet paste", while for precipitated RCs that were either dry or completely soaked with water the NMR label response showed a substantial line broadening.

Here we introduce a novel CP MAS NMR strategy to characterize the binding at the 1-C=O side of the Q$_A$ in comparison with the 1-^{13}C of the Q$_B$ in the ground state of the RC. First, two-dimensional (2-D) heteronuclear (^{1}H-^{13}C) dipolar correlation spectroscopy is used to investigate *R. sphaeroides* R26 RCs reconstituted with [1-^{13}C] UQ$_{10}$ for Q$_A$ or Q$_B$. From the heteronuclear correlation spectra, the isotropic chemical shifts of proton(s) that participate in polarization transfer to 1-^{13}C Q$_A$ or Q$_B$ are assigned by indirect detection of the proton response via a nearby ^{13}C label. In particular, hydrogen-bonded protons can be involved in a rapid magnetization buildup of a quaternary carbon [30]. Protons in a hydrogen bond typically resonate in the range of 8–15 ppm and can be identified from heteronuclear correlations. In a next step, Lee–Goldburg (LG) CP buildup curves are recorded from the [1-^{13}C] UQ$_{10}$ reconstituted RCs. From these buildup curves, the distances r_{CH} between the 1-^{13}C carbon and the proton(s) involved in the polarization transfer can be estimated [30].

2 Material and Methods

A batch of about 0.5 μmol Q$_A$ or Q$_B$-depleted *R. sphaeroides* R26 RCs was prepared following the procedures described in ref. 31. The quinones were removed by washing the RCs anaerobically for about 24 h with a solution of 4% lauryl-dimethylamine N-oxide (LDAO), 10 mM Tris (pH 8) and 10 mM *o*-phenanthroline on a (diethylamino)ethyl (DEAE) Sephacel column [32]. The RCs were rapidly reconstituted with 1-^{13}C UQ$_{10}$ obtained by total synthesis [33]. After removing from the column and desalting by dialysis, the samples were diluted to an OD of about 18 at a wavelength of 800 nm (OD$_{800}$) in 8 ml of solution of 0.025% LDAO, 10 mM Tris (pH 8) and 1 mM EDTA (TL buffer). To this RC solution, 460 μl [1-^{13}C] UQ$_{10}$ (1 mg/ml) in 1% Triton X-100 was added in three steps to a final concentration of 0.05%. After each step the RC-quinone mixture was allowed to incubate for 20 min at room temperature and the relative amounts of reconstituted Q$_A$ and Q$_B$ were determined by monitoring the recombination kinetics of the absorption changes at 865 nm following a flash of actinic light. The incorporation of Q$_A$ was close to 100%, while for about 30% of the RCs, [1-^{13}C] UQ$_{10}$ was also incorporated at the Q$_B$ position.

To remove both the labeled Q$_B$ and the denatured RCs, the mixture was diluted to a concentration of 3.5 μM in 150 ml of a 0.5% LDAO and 50 mM Tris (pH 8) solution. To reduce the RCs, solid NaBH$_4$ was added to a concentration of 5 mM. After incubating this solution for 10 min at room temperature,

the RCs were loaded on a DEAE Sephacel column and washed several times with a 0.5% LDAO and 50 mM Tris (pH 8) solution in order to remove re-leased Q_BH_2, traces of reduced UQ_{10}, denatured RCs, the Triton X-100 and the excess of $NaBH_4$. A salt gradient (0–500 mM NaCl) was applied to elute the RCs from the column at about 250 mM NaCl. After reconstitution the ratio of optical absorption at 280 and 800 nm is $A_{280}/A_{800} = 1.28$, which measures the quality of the sample.

The activity of the RCs following a flash of actinic light can be modeled with a single-exponential decay $A \cdot \exp(-t/\tau)$ with a decay constant $\tau = 0.108$ s, characteristic for the $P^+Q_A^{\cdot-} \to PQ_A$ back-reaction (Fig. 3a). The absence of a slowly decaying component with $\tau \approx 1$ s for the $P^+Q_B^{\cdot-}$ back-reaction implies that the excess of Q_B has been successfully removed by the reduction with $NaBH_4$. Figure 3b shows the kinetics of the same sample after adding a 5-fold excess of UQ_{10}. Since both the Q_A and Q_B sites are fully occupied in this prepa-ration, the decay is biexponential, $A_1 \cdot \exp(-t/\tau_1) + A_2 \cdot \exp(-t/\tau_2)$. From this mea-surement, the incorporation of Q_A is estimated as $A/(A_1 + A_2) \cdot 100\%$ and is found to be about 95%.

To prepare a sample for the NMR experiments, the NaCl was removed by dialyzing the RCs for 24 h at 4 °C against a 0.1% LDAO TL buffer, and two times 24 h against a 0.025% LDAO TL buffer. The RC solution was concen-trated using a 100 kDa filter (Amicon, Ca.) and superconcentrated to a volume of about 80 µl with a concentration of >1 mM by drying the preparation in a sealed container above a saturated salt solution at 4 °C. About 60 µl of this highly concentrated RC solution was used for the solid-state NMR experiments. During the concentration steps, and before and after the NMR experiment, ab-sorption spectra were monitored that confirmed a good quality of the sample.

For the preparation of the 1-^{13}C Q_B-labelled sample, about 0.4 µmol of RCs were diluted in 100 ml of a 0.5% LDAO and 50 mM Tris (pH 8) solution. Solid
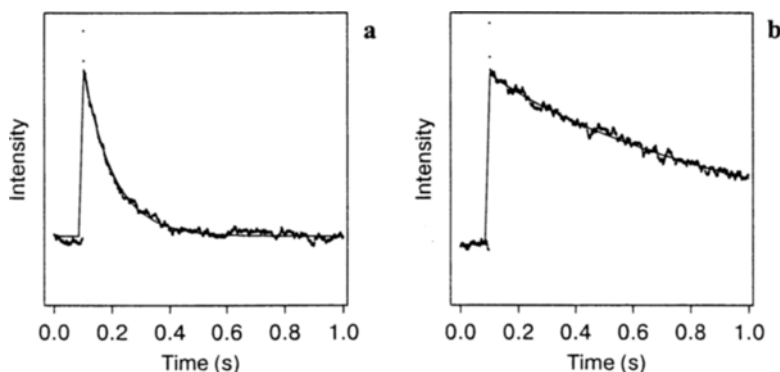

Fig. 3. Optical bleaching measured at 865 nm in RCs following a flash of actinic light before (a) and after (b) adding a 5-fold excess of UQ_{10}. The narrow lines represent single-exponential fits of the traces.

KBH_4 was added to a concentration of 5 mM to reduce the RCs. After incubating this solution for 10 min at room temperature, the RCs were loaded on a DEAE Sephacel column and were washed with a 0.5% LDAO, 50 mM Tris (pH 8) solution to remove the released Q_BH_2 and the excess of KBH_4. The Q_B-depleted RCs were eluted from the column with a 1 M NaCl (0.1% LDAO) solution and dialyzed overnight at 4 °C against a 0.025% LDAO TL buffer. A depletion of 10% in the Q_A and 90% in the Q_B was estimated from the recombination kinetics following a flash before and after adding a 5-fold excess of UQ_{10}.

Approximately 0.3 μmol of RCs with $[1-{}^{13}C]$ UQ_{10} for Q_B were prepared by adding a 5-fold excess of $[1-{}^{13}C]$ UQ_{10} to the Q_B-depleted RCs and allowing the RC-quinone mixture to incubate for one hour at room temperature and overnight at 4 °C. The reconstituted RCs were loaded on a DEAE Sephacel column, washed with 0.025% LDAO TL buffer to remove the excess of $[1-{}^{13}C]$ UQ_{10}, eluted with a 0.025% LDAO TL buffer containing 1 M NaCl, and dialyzed overnight at 4 °C against a 0.025% LDAO TL buffer. The RC solution was concentrated to >1 mM using a 100 kDa filter (Amicon, Ca.). After concentration, 85% of the RCs contained $[1-{}^{13}C]$ UQ_{10} at the Q_B side. Due to the 10% Q_A depletion before adding the $[1-{}^{13}C]$ UQ_{10}, up to 10% of the RCs will also be reconstituted with $[1-{}^{13}C]$ UQ_{10} for Q_A. From the $[1-{}^{13}C]$ Q_B RC preparation, about 0.2 μmol was used for the solid-state NMR experiments.

The NMR spectra were recorded using MSL-400 and DMX-600 spectrometers, equipped with 4 mm CP MAS probes (Bruker, Karlsruhe, Germany). The sample was confined to the center of the NMR coil by spacers in the rotor and a homebuilt controller was used to keep the spinning frequency constant to within a few hertz [34]. Two-pulse phase-modulation (TPPM) decoupling was used during data acquisition [35]. Low-temperature NMR measurements were performed using liquid-nitrogen-cooled bearing gas. The temperature of the bearing gas T_B was measured just before the gas entered the spinning assembly, and the temperature of the sample can be approximated by $T \approx 0.86 T_B + 50$ K (± 5 K) [36]. The detergent-solubilized samples were cooled down to 267 K at a relatively low spinning rate $\omega_r/2\pi \approx 1.5$ kHz. The freezing of the sample while spinning ensures a homogeneous sample distribution against the rotor wall.

2-D ^1H-^{13}C heteronuclear dipolar correlation spectra were recorded in a magnetic field of 14.1 T at ambient temperature. The correlation spectrum of the $[1-{}^{13}C]$ Q_A R26 RCs was obtained from hydrated-precipitated RCs [3], using the CP WISE technique with a short cross-polarization time of 200 μs [37]. In the t_1 dimension 32 points were collected. The correlation spectrum of hydrated-precipitated $[1-{}^{13}C]$ Q_B R26 RCs was recorded with frequency-switched LG (FSLG) ^1H homonuclear decoupling during the proton evolution [38]. A LG CP contact time of 4.5 ms was applied and 32 slices were recorded in t_1.

The LG CP buildup curves were obtained by the methods described in ref. 30. The spectrometer was set to the $n = -1$ Hartmann–Hahn matching condition. The ^{13}C signal intensities for the buildup curves were determined following the same procedure as described in ref. 3. The same phase correction was applied to all spectra in the polarization buildup series. The carbonyl region (190–

160 ppm) of the spectrum with the best signal-to-noise ratio for the 1-^{13}C UQ_{10} response was first deconvoluted with a superposition of two Gaussian lines, one for the label signal around 183 ppm and one for the natural-abundance peptide carbonyl background signal around 173 ppm. The isotropic chemical shifts and line widths were fixed at the values determined from this deconvolution. In this way, the integrated intensities of the label and carbonyl background signal are left as the only free parameters in the fit of the other spectra in the series, and they can be determined accurately.

3 Results

From 1-D ^{13}C CP MAS NMR spectra of hydrated-precipitated RCs, reconstituted with [1-^{13}C] UQ_{10} for Q_A, the [1-^{13}C] Q_A R26 RC resonance was assigned with a chemical shift of 183.8 ppm [3]. Figure 4 shows a contour plot of a 2-D ^{1}H-^{13}C heteronuclear dipolar correlation spectrum of hydrated-precipitated [1-^{13}C] Q_A RCs, recorded at ambient temperature, using an MAS rate $\omega_r/2\pi = 15.0$ kHz. The [1-^{13}C] Q_A resonance around 183.8 ppm has a correlation signal with a proton with $\sigma_i = 9.5 \pm 0.5$ ppm, indicated with an arrow in the 2-D correlation spectrum. This correlation signal predominantly involves intermolecular polarization transfer. The nearest protons in the UQ_{10} molecule are a proton of the nearby CH_2 moiety of the quinone tail ($r_{CH} = 0.27$ nm, [41]) and possibly one of the 6'-methoxy protons, depending on the orientation of the methoxy substituent. These protons all resonate more upfield and cannot account for the observed ^{1}H shift of about 9.5 ppm.
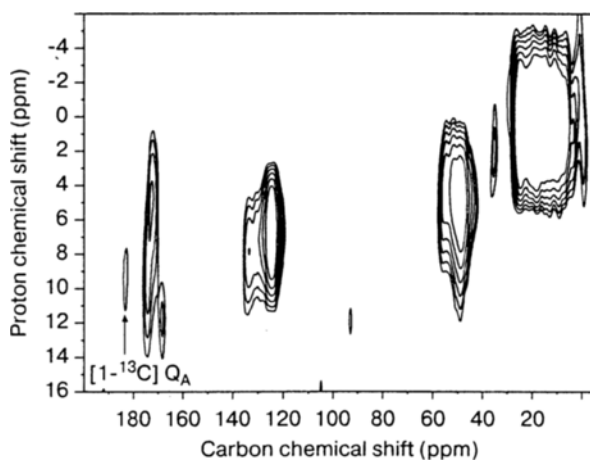

Fig. 4. Contour plot of a 2-D ^{1}H-^{13}C heteronuclear dipolar correlation spectrum of precipitated [1-^{13}C] Q_A R26 RCs, collected in a field of 14.1 T with the CP WISE technique. A spinning frequency of 15.0 kHz was applied. The arrow indicates the correlation signal with the ^{13}C label.
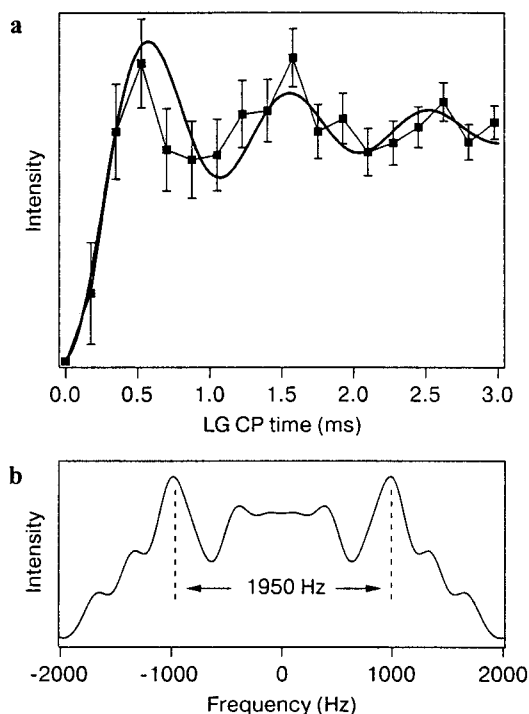
Fig. 5. LG CP buildup curve of [1-^{13}C] Q$_A$ (**a**) and its Fourier transform (**b**), recorded at T = 235 K from frozen detergent-solubilized [1-^{13}C] Q$_A$ R26 RCs. The data were acquired in a field of 9.4 T, using a spinning frequency of 11.0 kHz. The thick solid line in a represents a buildup curve simulated for a spin pair with CH distance r_{CH} = 0.2 nm.

Figure 5a shows a LG CP build-up curve of [1-^{13}C] Q$_A$, recorded from frozen detergent-solubilized [1-^{13}C] Q$_A$ R26 RCs at a temperature of 235 K in a magnetic field of 9.4 T. A MAS rate $\omega_r/2\pi$ = 11.0 kHz was used. The LG CP build-up curve is slowly oscillating, and its Fourier transform (Fig. 5b) provides the LG CP carbon spectrum with two resolved maxima. The build-up of the [1-^{13}C] Q$_A$ signal was compared with simulated build-up curves for CH spin pairs with different r_{CH}, which were taken from ref. 30. The best correspondence between the experimental and simulated data is found for a spin pair that has r_{CH} = 0.203 nm (Fig. 5a). Using the procedures described in ref. 30 to correlate the splitting $\Delta\omega/2\pi$ = 1950 Hz between the maxima in the Fourier transform in Fig. 5b to a distance r_{CH}, the 1950 Hz component translates into a short r_{CH} = 0.21±0.01 nm.

The NMR spectral characteristics of the [1-^{13}C] UQ$_{10}$ in the Q$_A$ site can be compared with the signals from the same label in the Q$_B$ site. Figure 6a shows a 1-D ^{13}C CP MAS NMR spectrum of frozen detergent-solubilized RCs, reconstituted with [1-^{13}C] UQ$_{10}$ for Q$_B$. The data were recorded at a temperature T = 244 K in a field of 9.4 T, and using a MAS rate $\omega_r/2\pi$ = 7.0 kHz. The as-
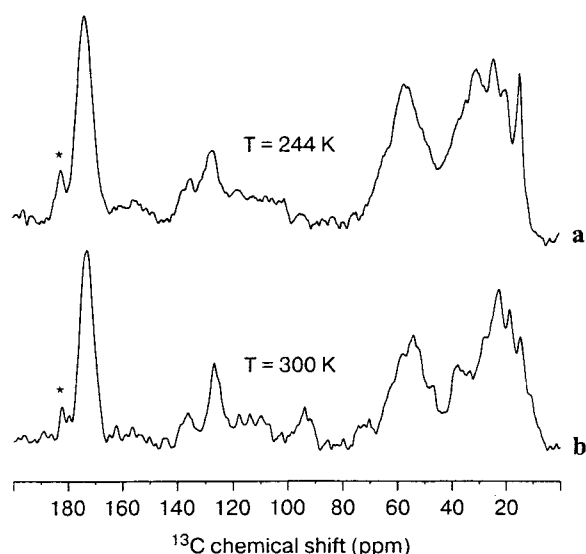
Fig. 6. 1-D CP MAS NMR spectra, recorded from frozen detergent-solubilized [1-^{13}C]Q_B R26 RCs at $T = 244$ K (a) and from hydrated-precipitated RCs at ambient temperature (b). The asterisk indicates the signal from the ^{13}C label. **a** Spectrum acquired in a field of 9.4 T, using a spinning frequency of 7.0 kHz. **b** Spectrum collected at 14.1 T with an MAS frequency of 12.0 kHz.

terisk indicates the response of the ^{13}C label. The [1-^{13}C] Q_B R26 RC signal resonates with a chemical shift of 182.4 ppm relative to TMS, which compares well with the shifts reported for [1-^{13}C] Q_A (183.8 ppm) and [4-^{13}C] Q_A (183.1 ppm, at $T = 190$ K) [3]. The Q_B signals are consistently broader than the corresponding resonances for the Q_A. A Gaussian line width of 300 Hz is measured for the [1-^{13}C] Q_B R26 RC response. The line width of the [1-^{13}C] Q_A signal is 150 Hz at room temperature and 250 Hz at $T = 230$ K, while for the [4-^{13}C] Q_A response a line width of 220 Hz is reported at $T = 190$ K [3]. The relatively large width of the [1-^{13}C] Q_B R26 RC signal suggests substantial heterogeneity in the chemical environment of the Q_B, more than for the Q_A. Figure 6b displays a ^{13}C CP MAS NMR spectrum of hydrated-precipitated [1-^{13}C] Q_B R26 RCs, collected at ambient temperature at a magnetic field of 14.1 T, using a MAS rate $\omega_r/2\pi = 12.0$ kHz. Also for the 1-^{13}C Q_B reconstituted preparation the precipitated RCs have essentially the same characteristics as the detergent-solubilized RCs. In particular, the chemical shift and line width are comparable, indicating that a good sample quality is maintained during the precipitation of the RCs.

A contour plot of a 2-D FSLG-decoupled heteronuclear (^{1}H-^{13}C) dipolar correlation spectrum of the precipitated [1-^{13}C] Q_B R26 RCs is shown in Fig. 7. The data were collected at room temperature with a MAS frequency $\omega_r/2\pi = 12.0$ kHz in a magnetic field of 14.1 T. The [1-^{13}C] Q_B at 182.4 ppm correlates with a proton signal around 9.5 ± 0.5 ppm, indicated with an arrow in the spectrum.
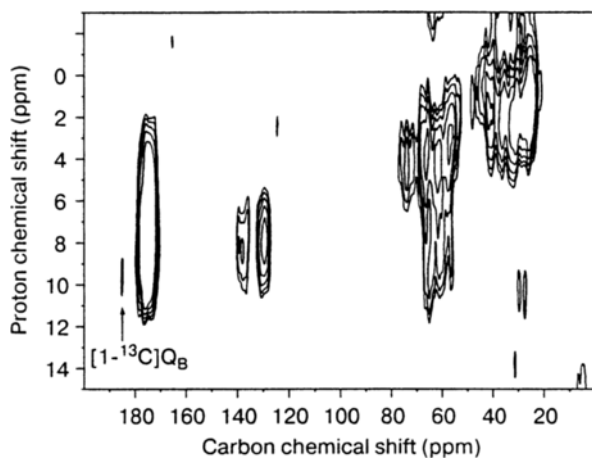
Fig. 7. Contour plot of a 2-D FSLG-decoupled heteronuclear (^{1}H-^{13}C) dipolar correlation spectrum of precipitated [1-^{13}C] Q_B R26 RCs, collected in a magnetic field of 14.1 T at room temperature. A spinning frequency of 12.0 kHz was used with an LG CP contact time of 4.5 ms. The arrow indicates the correlation signal with the ^{13}C label.
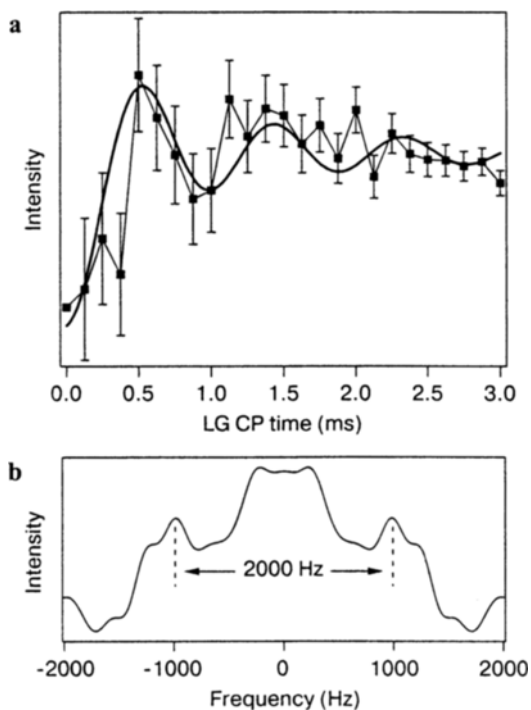

Fig. 8. LG CP buildup curve of [1-^{13}C] Q_B (**a**) and its Fourier transform (**b**), recorded at room temperature from hydrated-precipitated [1-^{13}C] Q_B R26 RCs. The data were acquired in a magnetic field of 14.1 T with a spinning frequency of 12.0 kHz. The thick solid line in **a** represents a buildup curve simulated for a spin pair with CH distance $r_{CH} = 0.2$ nm.

The downfield ^{1}H response provides strong evidence for intermolecular heteronuclear polarization transfer, similar to the [1-^{13}C] Q_A.

Finally, Fig. 8a shows the LG CP buildup curve recorded for the [1-^{13}C] Q_B in a preparation of hydrated-precipitated [1-^{13}C] Q_B R26 RCs at a field of 14.1 T, at ambient temperature. A spinning frequency $\omega_r/2\pi = 12.0$ kHz was applied. Using the same procedure as for the [1-^{13}C] Q_A, the buildup curve of the [1-^{13}C] Q_B signal can be compared with simulations of the LG CP process for isolated CH spin pairs. The best correspondence is found for a heteronuclear spin pair with a separation $r_{CH} = 0.196$ nm (Fig. 8a). From the analysis of the Fourier transform of the [1-^{13}C] Q_B signal buildup, a weak splitting $\Delta\omega/2\pi$ of about 2000 Hz is observed, which translates into a distance r_{CH} of approximately 0.21 nm.

4 Discussion

A number of 3-D structures of the *R. sphaeroides* RC, refined from X-ray diffraction data from crystallized RCs, have been reported in the literature [1, 23, 39–43]. According to X-ray data, the 1-C=O of Q_A can form a hydrogen bond to the backbone amide nitrogen of Ala M260, while for the proximal Q_B, X-ray suggests 1-carbonyl hydrogen bonds to the backbone amide nitrogen of Ile-L224 [1, 40, 42] or to the side chain oxygen of Ser-L223 [1, 39, 40]. However, recent FTIR studies indicate that Ser-L223 does not have a significant interaction with Q_B in the native RC. According to these investigations, the 1-C=O may form a multiple hydrogen bond with three different groups, the peptide NH of Ile-L224 and of Gly-L225 and the Ser-L223 hydroxyl group, allowing different groups to provide hydrogen bonds for distinct functions [26]. In this scenario, hydrogen bonds with backbone NH groups of Ile-L224 and Gly-L225 are most important for Q_B binding and to provide stability to the radical Q_B^- state [26].

From the ^{1}H-^{13}C heteronuclear correlation spectroscopy, it is found that both [1-^{13}C] Q_A and [1-^{13}C] Q_B have a correlation signal with a proton that resonates around 9.5 ppm (see Figs. 4 and 7). The ^{1}H shifts imply that the correlations arise from intermolecular polarization transfer, and the shifts are representative for hydrogen-bonded protons, for instance, a hydroxyl or amide proton in the protein environment. In contrast, a protonated 1-C=O is difficult to reconcile with the [1-^{13}C] chemical shift.

In addition, the CH distances between the ^{13}C label and the correlated protons are short, $r_{CH} = 0.21 \pm 0.01$ nm for both the [1-^{13}C] Q_A and the [1-^{13}C] Q_B. Such distances are very short for intermolecular transfer. Except for protons involved in hydrogen bonds, the shortest intermolecular distances between protons and carbons are of about 0.3 nm, since the molecular vibrations prevent in practice closer contacts. In contrast, hydrogen-bonding interactions involve the stabilization of orbital overlap between the atoms O and X involved in the hydrogen bond. In this way a short intermolecular distance between hydrogen-bonding partners is realized, in between the covalent bond $r_{OX} \leq 0.15$ nm, and the ionic bond $r_{OX} \geq 0.3$ nm.

Since both quinones are not protonated in the ground state, the proton that stabilizes the hydrogen bridge is bonded to the X-atom, which implies that $r_{XH} \sim 0.1$ nm [44]. Since we measure $r_{CH} = 0.21$ nm for both the Q_A and the Q_B, and the $r_{CO} = 0.12$ nm, our measurements indicate that in addition $r_{OH} \sim 0.1$ nm. This would imply a strong hydrogen bond for both quinones at the 1-C=O side, with $r_{OX} \sim 0.2$ nm. In such a strong hydrogen bond there is a single minimum in the proton potential energy, which favors a localization of the proton around the center of the bond [44]. In principle, weak interactions with distant protons can lead to a minor apparent shortening of the r_{CH} since it was demonstrated from model studies that the heteronuclear dipolar couplings to distant protons produce a minor increase of 100–200 Hz of the splitting $\Delta\omega/2\pi$ between the maxima in the LG CP carbon response of a strongly coupled CH pair [30]. However, we know from the 2-D heteronuclear correlation data that the contribution from the remote protons with different chemical shifts is small. For instance, there is not a strong correlation with the CH_2 protons at a distance of about 0.27 nm in the Q_A tail itself, resonating with a chemical shift in the range of about 1–4 ppm [41].

The observation of a short $r_{CH} = 0.21$ nm for both the Q_A and the Q_B provides evidence for a tight binding. For the Q_A, the 1-^{13}C signal builds up fast during the LG CP, which is only possible in the presence of at least one nearby proton (Fig. 5a). In the X-ray models, the Ala M260 N is positioned about 0.05–0.10 nm above the plane of the Q_A quinone ring, with the NH vector inclined at 45–60° with respect to the normal of the plane and directed towards the 1-carbonyl of Q_A [41, 42]. The shortest ^{1}H-^{13}C distance in the X-ray structural models from the 1-C=O is to the amide H of Ala M260 which is expected to resonate between 4 and 11 ppm, well in line with the NMR results [45]. The $r_{CH} = 0.21$ nm measured with the LG CP NMR appears less than the $r_{CH} \sim 0.25$ nm that transpires from the X-ray. Although the resolution of the X-ray is limited, this may indicate a structural displacement in the NMR preparation of the 1-C=O of the Q_A towards the Ala M260 NH in a tight hydrogen-bonding configuration that restricts the mobility with respect to the protein complex in the natural environment. There are other indications that the surfactant environment of the RCs affects the electronic structure of the cofactors [46]. Both the forward transfer and the $P^+Q_A^{\cdot-} \rightarrow PQ_A$ charge recombination have been found to be significantly faster in the native membrane than in detergent, while the free energy gap associated with the $Q_A^{\cdot-}Q_B \rightarrow Q_AQ_B^{\cdot-}$ electron transfer increases in the sequence of detergent → liposome → chromatophore system [47, 48]. These findings corroborate a subtle interplay between Q_A–protein interactions and the degree of hydration of the RCs, which may explain the symmetry reversal with respect to the FTIR and EPR observed through the pronounced effects on the CP efficiency and line width of the NMR response of the Q_A [4].

The narrow line for the [1-^{13}C] response of the Q_A is in line with a well-defined binding environment, while the broader [1-^{13}C] response for the Q_B side indicates that a structural heterogeneity is not necessarily accompanied by weaker binding interactions, in line with the FTIR studies and X-ray data for the proxi-

mal site that favor a structure with the C1 carbonyl group of the Q_B involved in three hydrogen bonds in parallel [23, 26]. The $r_{CH} \sim 0.2$ nm for the 1-C=O Q_B is similar to the Q_A, reflecting strong interaction with a hydrogen-bonding partner. Since the CP proceeds through the dipolar interactions, the shortest r_{CH} will have the strongest dipolar coupling and will contribute most to the signal intensity in the CP heteronuclear correlation transfer processes. The hydrogen bonding structure for the 1-C=O of the Q_B appears static on the scale of the NMR since dynamics would have scaled the dipolar coupling leading to apparently longer distance.

Acknowledgments

References

1. Allen J.P., Feher G., Yeates T.O., Komiya H., Rees C.D.: Proc. Natl. Acad. Sci. USA **85**, 8487–8491 (1988)
2. Feher G., Allen J.P., Okamura M.Y., Rees D.C.: Nature **339**, 111–116 (1989)
3. van Liemt W.B.S., Boender G.J., Gast P., Hoff A.J., Lugtenburg J., de Groot H.J.M.: Biochemistry **34**, 10229–10236 (1995)
4. van Rossum B.J., van Liemt W.B.S., Boender G.J., Gast P., Hoff A.J., Lugtenburg J., de Groot H.J.M. in: Photosynthesis: From Light to Biosphere; Xth International Photosynthesis Congress, Montpellier, France, 1995. (Mathis P., ed.), vol. 1, p. 899. Dordrecht: Kluwer Academic 1995.
5. Feher G., Isaacson R.A., Okamura M.Y., Lubitz W. in: Antennas and Reaction Centers of Photosynthetic Bacteria (Michel-Beyerle M.E., ed.). Springer Series in Chemical Physics, vol. 42, p. 174. Berlin: Springer 1985.
6. Lubitz W., Abresch E.C., Debus R.J., Isaacson R.A., Okamura M.Y., Feher G.: Biochim. Biophys. Acta **808**, 464–469 (1985)
7. van den Brink J., Spolyakov A., van Liemt W.B.S., Raap J., Lugtenburg J., Gast P., Hoff A.J.: FEBS Lett. **353**, 273–276 (1994)
8. van den Brink J.S., Hulsebosch R.J., Gast P., Hore P.J., Hoff A.J.: Biochemistry **33**, 13668–13677 (1994)
9. Isaacson R.A., Abresch E.C., Lendzian F., Boullais C., Paddock M.L., Mioskowski C., Lubitz W., Feher G.: Biophys. J. **69**, 311–322 (1995)
10. Bosch M.K., Gast P., Hoff A.J., Spoyalov A.P., Tsvetkov Yu.D.: Chem. Phys. Lett. **239**, 306–312 (1995)
11. Hulsebosch R.J.: Ph.D. thesis, Leiden University, Leiden, The Netherlands (1999)
12. Rohrer M., Gast P., Möbius K., Prisner T.F.: Chem. Phys. Lett. **259**, 523–530 (1996)
13. Brudler R., de Groot H.J.M., van Liemt W.B.S., Steggerda W.F., Esmeijer R., Gast P., Hoff A.J., Lugtenburg J., Gerwert K.: EMBO J. **13**, 5523–5530 (1994)
14. Breton J., Boullais C., Burie J.R., Nabedryk E., Mioskowski C.: Biochemistry **33**, 14378–14386 (1994)
15. Brudler R., de Groot H.J.M., van Liemt W.B.S., Gast P., Hoff A.J., Lugtenburg J., Gerwert K.: FEBS Lett. **370**, 88–92 (1995)
16. Breton J., Boullais C., Berger G., Mioskowski C., Nabedryk E.: Biochemistry **34**, 11606–11616 (1995)
17. Kleinfeld D., Okamura M.Y., Feher G.: Biochemistry **23**, 5780–5786 (1984)

18. Peloquin J.M., Williams J.C., Lin X., Alden R.G., Taguchi A.K.W., Allen J.P., Woodbury N.W.: Biochemistry 33, 8089–8100 (1994)
19. Holzwarth A.R., Müller M.G.: Biochemistry 35, 11820–11831 (1996)
20. Parson W.W., Chu Z.T., Warshel A.: Biophys. J. 74, 182–191 (1998)
21. Cohen B.E., McAnaney T.B., Park E.S., Jan Y.N., Boxer S.G., Jan L.Y.: Science 296, 1700–1703 (2002)
22. Nagy L., Milano F., Dorogi M., Agostiano A., Laczko G., Szebenyi K., Varo G., Trotta M., Maroti P.: Biochemistry 43, 12913–12923 (2004)
23. Stowell M.B.H., McPhillips T.M., Rees D.C., Soltis S.M., Abresch E., Feher G.: Science 276, 812–816 (1997)
24. Graige M.S., Feher G., Okamura M.Y.: Proc. Natl. Acad. Sci. USA 95, 11679–11684 (1998)
25. Breton J., Boullais C., Mioskowski C., Sebban P., Baciou L., Nabedryk E.: Biochemistry 41 12921–12927 (2002)
26. Nabedryk E., Paddock M.L., Okamura M.Y., Breton J.: Biochemistry 44, 14519–14527 (2005)
27. Breton J., Wakeham M.C., Fyfe P.K., Jones M.R., Nabedryk E.: Biochim. Biophys. Acta 1656, 127–138 (2004)
28. Breton J.: Biochemistry 43, 3318–3326 (2004)
29. Boers R.B., Gast P., Hoff A.J., de Groot H.J.M., Lugtenburg J.: Eur. J. Org. Chem. 1, 189–202 (2002)
30. Rossum B.J., de Groot C., de Groot H.J.M., Ladizhansky V., Vega S.: J. Am. Chem. Soc. 122, 3465–3472 (2000).
31. Feher G., Okamura M.Y. in: The Photosynthetic Bacteria (Clayton R.K., Sistrom W.R., eds.), pp. 349–386. New York: Plenum 1978.
32. Okamura M.Y., Isaacson R.A., Feher G.: Proc. Natl. Acad. Sci. USA 72, 3491–3495 (1975)
33. van Liemt W.B.S., Steggerda W.F., Esmeijer R., Lugtenburg J.: Rec. Trav. Chim. Pays-Bas 113, 153–161 (1994)
34. de Groot H.J.M., Copié V., Smith S.O., Allen P.J., Winkel C., Lugtenburg J., Herzfeld J., Griffin R.G.: J. Magn. Reson. 77, 251–257 (1988)
35. Bennet A.E., Rienstra C.M., Auger M., Lakshmi K.V., Griffin R.G.: J. Chem. Phys. 103, 6951–6957 (1995)
36. Fischer M.R., de Groot H.J.M., Raap J., Winkel C., Hoff A.J., Lugtenburg J.: Biochemistry 31, 11038–11049 (1992)
37. Schmidt-Rohr K., Spiess H.: Multidimensional Solid State NMR and Polymers. London: Academic Press 1994.
38. van Rossum B.J., Förster H., de Groot H.J.M.: J. Magn. Reson. 124, 516–519 (1997)
39. Chang C.H., El-Kabbani O., Tiede D., Norris J., Schiffer M.: Biochemistry 30, 5352–5360 (1991)
40. Chirino A.J., Lous E.J., Huber M., Allen J.P., Schenck C.C., Paddock M.L., Feher G., Rees D.: Biochemistry 33, 4584–4593 (1994)
41. Ermler U., Fritzsch G., Buchanan S.K., Michel H.: Structure 2, 925–936 (1994)
42. Arnoux B., Gaucher J.F., Ducruix A., Reiss-Husson F.: Acta Crystallogr. D 51, 368–379 (1995)
43. Arnoux B., Reiss-Husson F.: Eur. Biophys. J. 24, 233–242 (1996)
44. Limbach H.H., Manz J.: Ber. Bunsenges. Phys. Chem. Chem. Phys. 102, 289–291(1998)
45. Seavey B.R., Farr E.A., Westler W.M., Markley J.L.: J. Biomol. NMR 1, 217–236 (1991)
46. Muh F., Rautter J., Lubitz W.: Biochemistry 36, 4155–4162 (1997)
47. Nagy L., Fodor E., Tandori J., Rinyu L., Farkas T.: Aust. J. Plant Physiol. 25, 465–473 (1999)
48. Taly A., Baciou L., Sebban P.: FEBS Lett. 532, 91–96 (2002)

Authors' address: Huub J. M. de Groot, Gorlaeus Laboratories, Leiden Insitute of Chemistry, Leiden University, POB 9502, 2300 RA Leiden, The Netherlands
E-mail: ssnmr@chem.leidenuniv.nl